Journal of Experimental Botany, Vol. 63, No. 10, pp. 3815–3828, 2012
doi:10.1093/jxb/ers074 Advance Access publication 20 March, 2012
This paper is available online free of all access charges (see http://jxb.oxfordjournals.org/open_access.html for further details)

Journal of Experimental Botany
www.jxb.oxfordjournals.org

RESEARCH PAPER

Auxin transport at cellular level: new insights supported by mathematical modelling

Petr Hošek[1,2,*], Martin Kubeš[1,*], Martina Laňková[1], Petre I. Dobrev[1], Petr Klíma[1], Milada Kohoutová[2], Jan Petrášek[1], Klára Hoyerová[1,†], Marcel Jiřina[2] and Eva Zažímalová[1]

[1] Institute of Experimental Botany, the Academy of Sciences of the Czech Republic, Rozvojová 263, 165 02 Prague 6, Czech Republic
[2] Department of Biomedical Informatics, Faculty of Biomedical Engineering, Czech Technical University in Prague, Nám. Sítná 3105, 272 01 Kladno 2, Czech Republic

* These authors contributed to this paper equally.
† To whom correspondence should be addressed. E-mail: hoyerova@ueb.cas.cz

Received 3 December 2011; Revised 1 February 2012; Accepted 16 February 2012

Abstract

The molecular basis of cellular auxin transport is still not fully understood. Although a number of carriers have been identified and proved to be involved in auxin transport, their regulation and possible activity of as yet unknown transporters remain unclear. Nevertheless, using single-cell-based systems it is possible to track the course of auxin accumulation inside cells and to specify and quantify some auxin transport parameters. The synthetic auxins 2,4-dichlorophenoxyacetic acid (2,4-D) and naphthalene-1-acetic acid (NAA) are generally considered to be suitable tools for auxin transport studies because they are transported specifically via either auxin influx or efflux carriers, respectively. Our results indicate that NAA can be metabolized rapidly in tobacco BY-2 cells. The predominant metabolite has been identified as NAA glucosyl ester and it is shown that all NAA metabolites were retained inside the cells. This implies that the transport efficiency of auxin efflux transporters is higher than previously assumed. By contrast, the metabolism of 2,4-D remained fairly weak. Moreover, using data on the accumulation of 2,4-D measured in the presence of auxin transport inhibitors, it is shown that 2,4-D is also transported by efflux carriers. These results suggest that 2,4-D is a promising tool for determining both auxin influx and efflux activities. Based on the accumulation data, a mathematical model of 2,4-D transport at a single-cell level is proposed. Optimization of the model provides estimates of crucial transport parameters and, together with its validation by successfully predicting the course of 2,4-D accumulation, it confirms the consistency of the present concept of cellular auxin transport.

Key words: Auxin metabolism, auxin transport, auxin transport inhibitors, 2,4-D, mathematical modelling, tobacco BY-2 cells.

Introduction

Auxin is a signal molecule that is present in plant tissues in nanomolar concentrations (Davies, 2010). A fast and tight control of auxin levels is necessary for the proper regulation of plant growth and development and for responses to environmental stimuli. Such control is realized via two basic processes: auxin metabolism, and its transport within and between cells. Auxin metabolism, including biosynthesis, conjugation, de-conjugation and degradation (Normanly *et al.*, 2010; Ludwig-Müller, 2011), as well as intracellular distribution (Mravec *et al.*, 2009; Tromas *et al.*, 2010) and intercellular distribution (Petrášek and Friml, 2009; Peer *et al.*, 2011) determine the availability of auxin for its transporters (facilitators) in the plasma membrane (PM). The numbers and activities of auxin transporters determine the directional flow of auxin through plant tissues (Zažímalová *et al.*, 2010; Leyser, 2011).

The physical-chemical nature of auxin molecules underlies the mechanism of their transport across the PM. Since auxins are weak acids, the degree of their dissociation depends on pH. Intracellular (cytoplasmic) pH in plant cells is approximately 7, resulting in the almost complete dissociation of auxin molecules and thus providing basis

for trapping auxin anions inside cells as anions can only be excreted through an (always limited) number of PM-located facilitators. These facilitators, postulated to be localized asymmetrically on the PM, together with passive diffusive auxin uptake can mediate polar auxin transport through the tissue ('chemiosmotic hypothesis': Rubery and Sheldrake, 1974; Raven, 1975; Goldsmith, 1977).

Although there is no need for active auxin transporters according to the chemiosmotic hypothesis, there are several types of transport proteins with specific features. Proteins of the AUX1/LAX subfamily of PM amino acid permeases (Parry *et al.*, 2001*b*) play a role in active auxin influx as well as some of the ABCB pumps such as CjMDR1/ABCB1 (Shitan *et al.*, 2003) or ABCB4 (Terasaka *et al.*, 2005; Cho *et al.*, 2007). Moreover, it was indicated (Yang and Murphy, 2009) and recently confirmed (Kubeš *et al.*, 2012) that ABCB4 functions as the auxin concentration-driven influx/efflux transporter. The efflux of auxin, on the other hand, is mediated by transporters from the PIN protein family as well as by ABCB1, ABCB19 and the above-mentioned ABCB4 under different conditions (Geisler and Murphy, 2006; Petrášek and Friml, 2009; Titapiwatanakun and Murphy, 2009; Zažímalová *et al.*, 2010). Collectively, all the transporters are indispensable for various developmental events, for example, cell elongation, pattern formation or shoot and root branching (see review by Petrášek and Friml, 2009).

A dominant factor responsible for the co-ordination of these developmental events is the emergence and maintaining of cell polarity that is determined by the asymmetrical distribution of PIN efflux carriers over the surface of the cell (Gälweiler *et al.*, 1998). However, the precise molecular nature of the mechanism controlling PIN localization on the PM is neither entirely clarified nor experimentally proven yet. For this reason, several mathematical models have recently been proposed in order to examine the numerous hypotheses on PIN localization and the mechanism of cell polarity establishment.

One of the well-known processes co-ordinated through auxin transport regulation is the initiation of vein formation. It was addressed by Sachs (1969), who proposed a plausible scenario how auxin-conductive channels of polarized cells could form in undifferentiated tissue, thus preceding and determining the formation of vasculature. His canalization hypothesis suggested a positive feedback between the flow of a signal molecule (auxin) and the capacity of its flow. This concept, later formulated mathematically by Mitchison (1980*a*) and Mitchison *et al.* (1981), formed the basis for future mathematical models that suggested re-localization of PIN1 efflux carriers in response to auxin flow (Feugier *et al.*, 2005; Fujita and Mochizuki, 2006).

Another principle of auxin transport regulation was often implemented to construct models capable of reproducing the specific patterns of auxin concentration maxima in the surface layer of the shoot apical meristem during phyllotaxis. In these models, auxin concentration in adjacent cells was usually used as the signal modulating carrier localization (Jönsson *et al.*, 2006; Smith *et al.*, 2006).

The suggested existence of these two regulatory mechanisms based on different signals (auxin flow and auxin concentration) raised the question about their possible integration or replacement by a single one (Smith and Bayer, 2009; Garnett *et al.*, 2010). Consequently, several models emerged attempting to find a unifying auxin-related mechanism that modulates the localization of PINs (Merks *et al.*, 2007; Stoma *et al.*, 2008; Bayer and Smith *et al.*, 2009). Later on, more mechanisms and hypotheses were implemented into computational studies of auxin transport and the regulation of its polarity. These include hypothetical auxin receptors diffusible through the cell wall (Wabnik *et al.*, 2010), effects of the tissue mechanics and the resulting mechanical stresses on PIN localization (Heisler *et al.*, 2010), and auxin-induced cell wall acidification (Steinacher *et al.*, 2012).

As mentioned above, these models focus mainly on testing hypotheses. This fact may be accompanied by several issues. First, cell representation may be considerably simplified, for example, by omitting cell wall compartments (Stoma *et al.*, 2008; Bayer and Smith *et al.*, 2009) as originally proposed by Mitchison (1980*b*) and discussed by Kramer (2008) and/or by neglecting inner cell compartments (Merks *et al.*, 2007; Wabnik *et al.*, 2011). Second, the parameter values may be arbitrary (Feugier *et al.*, 2005), adopted from different systems (Steinacher *et al.*, 2012) or estimated roughly (Heisler and Jönsson, 2006). Third, the models mostly lack computationally exploitable experimental data. Obviously, some of these shortcomings and limitations can be resolved by further research into cellular auxin transport enhanced by data-driven mathematical modelling aimed at characterizing the components of auxin transport in detail and specifying their parameters.

The relative contributions of auxin influx and auxin efflux transporters were investigated in the past using a cell-based system relying on different substrate specificities of the respective carriers (Delbarre *et al.*, 1996). Competition experiments on auxin influx or efflux, which were performed using externally applied radiolabelled tracer and a non-labelled competitor, revealed saturable components involved in the uptake of 2,4-dichlorophenoxy acetic (2,4-D) and the native indole-3-acetic acid (IAA) as well as in the efflux of IAA and naphthalene-1-acetic acid (NAA).

Besides the non-labelled competitors, specific auxin transport inhibitors can be used to separate the influx and efflux activities. Inhibitors of auxin influx carriers include the synthetic compounds 1-naphthoxyacetic acid (1-NOA), 2-naphthoxyacetic acid (2-NOA), 3-chloro-4-hydroxyphenylacetic acid (CHPAA), and the natural chromosaponin (Imhoff *et al.*, 2000; Rahman *et al.*, 2001; Laňková *et al.*, 2010). Inhibitors of auxin efflux carriers include synthetic phytotropins 1-naphthylphthalamic acid (NPA), 2-(1-pyrenoyl)benzoic acid (PBA), cyclopropyl propane dione (CPD), 2,3,5-triiodobenzoic acid (TIBA), and natural flavonoids (Rubery, 1990; Petrášek *et al.*, 2003; Peer and Murphy, 2007).

In general, it was postulated that NAA enters cells predominantly by diffusion and its accumulation level is controlled by efflux carriers (Delbarre *et al.*, 1996). By contrast, 2,4-D was transported into the cells mainly by influx carriers and it was found to be a substrate for auxin efflux carriers only at concentrations above 100 μM. Natural auxin IAA was shown to be a substrate for both types of carriers as

well as being able to enter cells passively in considerable amounts. Similar auxin transport characteristics were subsequently confirmed in *Arabidopsis* root cells of the *aux1-7* mutant deficient in auxin influx carrier (Yamamoto and Yamamoto, 1998; Parry *et al.*, 2001*a*; Rahman *et al.*, 2001). Using these data, Kramer and Bennett (2006) calculated that the contribution of carrier-mediated uptake is about 10-times higher than uptake by diffusion in *Arabidopsis* root cells.

Besides the transport of auxin, Delbarre *et al.* (1996) also addressed auxin metabolism and showed that, in tobacco Xanthi XHFD8 cells, NAA was metabolized during a 15 min incubation to one dominant metabolite, assumed to be a glucose ester conjugate, while 2,4-D remained non-metabolized during the test period. IAA metabolism was approximately two times slower compared with NAA metabolism in Xanthi cells.

The work by Delbarre *et al.* (1996) still presents the most elaborated experimentally derived cellular concept of auxin transport characterization, even though the present analytical methods render some of the results outdated. The potential of mathematical analysis of the accumulation data had not been fully utilized there, as only a rough mathematical wireframe, that was not defined as a proper model, was used. The variety of auxin transport inhibitors available at present is also considerably broader and better characterized: in particular, the specific auxin influx inhibitor CHPAA represents a substantial improvement over their system that lacked a feasible influx inhibitor. Finally, the auxin metabolic profiles determined by TLC at Delbarre *et al.* (1996) should be considered for revision using more advanced methods, such as HPLC and/or MS.

The goal of this work is to describe auxin transport pathways at the cellular level more comprehensively, using the following combination of experimental and theoretical approaches. (i) The updated methodology of the measurement of accumulation of radiolabelled auxins in tobacco BY-2 cell suspensions. (ii) HPLC metabolic profiling of auxins in cells and media during the time span of the accumulation experiments and successive analysis of the metabolites (GC-MS). (iii) The construction of a data-driven mathematical model of cellular auxin transport in order to validate the experimental results.

Our experimental data, directly supported by the consequently derived mathematical model of the cellular transport of 2,4-D, provide new insight into the metabolism and transport of NAA and 2,4-D and further reveal the parameters of 2,4-D transport that are consistent with the auxin transport characteristics observed earlier.

Materials and methods

Plant material

Cells of tobacco line BY-2 (*Nicotiana tabacum* L. cv. Bright Yellow-2; Nagata *et al.*, 1992) were cultured in a liquid medium containing 3% (w/v) sucrose, 4.3 g l^{-1} Murashige and Skoog salts, 100 mg l^{-1} inositol, 1 mg l^{-1} thiamine, 0.2 mg l^{-1} 2,4-D, and 200 mg l^{-1} KH_2PO_4; pH 5.8. Cells of tobacco line Xanthi (*Nicotiana tabacum* L. cv. Xanthi XHFD8; Muller *et al.*, 1985) were cultured in Gamborg B5 liquid medium (Gamborg *et al.*, 1968) containing 0.176 mg l^{-1} 2,4-D and 0.1 mg l^{-1} kinetin. Both cell lines were cultured in darkness at 26 °C on an orbital incubator (Sanyo Gallenkamp, Schöller Instruments Inc., Prague, Czech Republic) at 150 rpm and 32 mm orbit, and subcultured weekly. Stock BY-2 and Xanthi calli were maintained on media solidified with 0.6% (w/v) agar and subcultured monthly.

Chemicals

3-chloro-4-hydroxyphenylacetic acid (CHPAA), 2,4-dichlorophenoxy acetic acid (2,4-D) and all commonly used chemicals were supplied by Sigma-Aldrich, Inc. (St Louis, USA) and Duchefa (Haarlem, The Netherlands). 1-naphthylphthalamic acid (NPA) was supplied by OlChemIm Ltd. (Olomouc, Czech Republic). ^{3}H-benzoic acid (^{3}H-BeA [4^{3H}]) and ^{3}H-2,4-dichlorophenoxyacetic acid (^{3}H-2,4-D) (both of specific radioactivity 20 Ci $mmol^{-1}$), as well as ^{3}H-naphthalene-1-acetic acid (^{3}H-NAA) (specific radioactivity 25 Ci $mmol^{-1}$) were supplied by American Radiolabeled Chemicals, Inc. (St Louis, USA).

Auxin accumulation assays

Auxin accumulation in 2-d-old cells was measured according to Delbarre *et al.* (1996) as adapted for BY-2 cells by Petrášek *et al.* (2003). Two minutes before the beginning of the accumulation assay (i.e. addition of labelled auxin), if required, the inhibitors CHPAA, NPA or their combination were added from 50 mM dimethyl sulphoxide (DMSO) stock solutions to give a final concentration of 10 μM. Radiolabelled auxins (^{3}H-2,4-D or ^{3}H-NAA) were added to give a 2 nM final concentration. 0.5 ml aliquots of cell suspension were collected every 10 s (approximately 60 samples per one run) and accumulation of the label was terminated by rapid filtration under reduced pressure on 22 mm diameter cellulose filters. The cell cakes on filters were transferred to scintillation vials, extracted with 0.5 ml of 96% ethanol for 30 min, followed by the addition of 4 ml of scintillation solution (EcoLite Liquid Scintilation Fluid, MP Biomedicals, Solon, USA). Radioactivity was determined by liquid scintillation counting with automatic correction for quenching (Packard Tri-Carb 2900TR, Packard-Canberra, Meridian, CT, USA). The results of auxin accumulation were expressed as pmols of particular auxin accumulated per 10^{6} cells. All treatments were done in at least three biological repetitions.

HPLC metabolic profiling

Two-day-old tobacco BY-2 or Xanthi cells were prepared for experiments by equilibration with the uptake buffer as described above for the accumulation assays (Delbarre *et al.,* 1996). Experiments were performed in the uptake buffer under standard cultivation conditions. After the addition of ^{3}H-BeA, ^{3}H-NAA or ^{3}H-2,4-D (final concentration 20 nM), the cells were incubated for 0, 10 or 20 min. Cells and cultivation medium (uptake buffer in this case) were collected and frozen in liquid nitrogen (200 mg of fresh weight of cells and 10 ml medium per sample). Extraction and purification of auxin metabolites were performed as described (Dobrev and Kamínek, 2002; Dobrev *et al.*, 2005). The metabolites were separated on HPLC consisting of a series 200 autosampler, lc pump, and a 235C diode array detector (Perkin Elmer, Shelton, USA) using a Luna C18(2) 150×4.6 mm, 3 μm column (Phenomenex, Torrance, USA), mobile phase A: 40 mM CH_3COONH_4, (pH 4.0) and mobile phase B: CH_3CN/CH_3OH, 1/1, (v/v). The flow rate was 0.6 ml min^{-1} with linear gradient 30–50% B for 10 min, 50–100% B for 1 min, 100% B for 2 min, and 100–30% B for 1 min. The column eluate was monitored with 235C DAD followed by a Ramona 2000 flow-through radioactivity detector (Raytest GmbH, Straubenhardt, Germany) after online mixing with three volumes (1.8 ml min^{-1}) of liquid scintillation cocktail (Flo-Scint III, Perkin Elmer). The radioactive metabolites were identified on the basis of a comparison of their retention times

with authentic standards. For the presentation of results, the total integrated area of chromatogram plots was normalized based on the equalization of total accumulated radiolabel.

Identification of the unknown NAA metabolite

Tobacco BY-2 cells were incubated with 10 μM NAA for 2 h. The main NAA metabolite M1 (retention time 15 min) was purified as for the metabolite profiling of radioactive NAA above. M1 was then applied to LC-ESI-MS/MS, which consisted of HPLC Ultimate 3000 (Dionex, Sunnyvale, USA) coupled to a hybrid triple quadrupole/linear ion trap 3200 Q TRAP (AB Sciex, Foster City, USA). MS was set at negative mode. Solution of M1 in 1 mM CH_3COOH in 50% methanol was infused into MS and full-scan mass spectra, and product ion and precursor ion scans were recorded. To study the stability of M1 under mild alkaline conditions, the M1 was poured into 0.1 M NH_4OH and incubated at room temperature. Every 5 min, an aliquot was injected into the LC/MS separated on column Luna C18(2)-HST, 50×3 mm, 2.5 μm (Phenomenex, Torrance, USA), isocratic 60% A: 2 mM CH_3COOH and 40% B: CH_3CN at 0.3 ml min^{-1} flow rate. MS was set at multiple reaction monitoring mode with records of Q1>Q3 transitions of NAA (185>141), M1 (347>141), glucose (179>89), and 2,4-D (219>161, internal standard). The main BeA metabolite (retention time 2.52 min) was similarly identified.

Mathematical modelling

The mathematical model of 2,4-D transport between the intracellular and extracellular environment was defined and mathematically formulated by a set of differential equations for each experimental setup (various inhibitor combination, see Figs 3 and 4). These sets were analytically solved for intracellular concentration, giving a formula of a function describing the time-course of 2,4-D concentration inside the cell. Using ^{3}H-2,4-D accumulation data measured under the effect of inhibitors (CHPAA, NPA or both CHPAA and NPA), parameter optimization was then performed by altering parameter values in order to minimize the value of objective function defined as summed squares of residuals (differences between measured and simulated values of intracellular 2,4-D concentration). Each set of parameters was used to simulate all experimental variants (all inhibitor combinations and repetitions) at a time, and all squared residuals were summed with equal weights to obtain a single value of the objective function. Since the objective function had many local minima, the optimization problem was solved using the following combination of gradient-based and enumerative numerical methods. Over three million of the initial parameter sets were randomly generated within the probable parameter value range, and from all these starting points a gradient-based optimization algorithm was initiated. From the results obtained here, the set of parameters appropriate for the deepest found minimum of the objective function was then declared to be the final parameter estimate. The acquired parameter estimates were then used to simulate the course of inhibitor-free ^{3}H-2,4-D accumulation (control) in order to validate the model. Sensitivity analysis was performed by plotting the relative change of the objective function value against the relative change of the value of each parameter, while the other parameters remained constant at their optimal estimates. Resulting curves, therefore, represent sections through the objective function near its minimum. All calculations were performed using the MATLAB software package (The MathWorks Inc., Natick, MA, USA).

Results

2,4-D as a tool for probing cellular auxin transport

To evaluate auxin transport at the cellular level, the mathematical model has to take into account not only passive diffusion, active influx, and active efflux of auxin molecules, but also their metabolic conversions. Therefore, the rate of metabolism was determined in BY-2 cells of the synthetic auxins 2,4-D and NAA, which are widely used to track auxin influx and efflux, respectively. Conversion of ^{3}H-NAA into the corresponding metabolites occurred almost immediately (within a few seconds) after ^{3}H-NAA addition to the cell suspension (Fig. 1A). One major metabolite M1 (see Supplementary Figs S3 and S4 at *JXB* online) covering approximately 50% of total radioactivity and five minor metabolites were observed. Importantly, no significant amount of any metabolite was found in the incubation medium. This observation indicates that products of NAA metabolism, including the predominant metabolite M1, are unable to translocate across the PM and therefore remain inside the cells. The major metabolite, M1, was identified as naphthalene-1-acetic acid-glucosyl-ester (NAA-Glc) (more details of NAA metabolism are given in Fig. 1A for BY-2 and in Supplementary Fig. S1A at *JXB* online for Xanthi).

In contrast to NAA, metabolism of 2,4-D in BY-2 cells was fairly slow. Compared with the rapid metabolic conversion of NAA to the one predominant metabolite, NAA-Glc, 2,4-D was only partially metabolized to minor amounts of three unknown metabolites as the relative levels of ^{3}H-2,4-D decreased slightly during the 20 min incubation with a parallel increase of one of the minor metabolites (Fig. 1B; see Supplementary Fig. S1B at *JXB* online). Relative levels of ^{3}H-2,4-D in the incubation medium remained constant and only traces of its three metabolites were observed, indicating that the products of 2,4-D metabolism remain mainly inside cells, similarly to metabolites of other weak acids tested (Fig. 1B; see Supplementary Fig. S1B at *JXB* online).

Altogether, 2,4-D is much more resistant to metabolic conversions compared with NAA or BeA (Fig. 1C; see Supplementary Fig. S1C at *JXB* online), thus making 2,4-D a promising tool for probing the characteristics of cellular auxin transport and offering an opportunity for the application of mathematical modelling based on quantitative data.

Characterization of the dynamics of 2,4-D transport at the cellular level

Since the metabolism of 2,4-D in BY-2 cells is negligible during 10 min of application and thus does not significantly affect the intracellular 2,4-D concentration, the dynamics of 2,4-D transport was investigated in these cells using accumulation assays within this limited time span. The cells rapidly accumulated ^{3}H-2,4-D from the media, with gradually decreasing accumulation speed as the fluxes in both directions (into and out of cells) were equilibrating (Fig. 2A).

Since 2,4-D is a good substrate for auxin influx carriers (Delbarre *et al.*, 1996) it was not surprising that CHPAA—a specific auxin influx inhibitor (Imhoff *et al.*, 2000, Laňková *et al.*, 2010)—effectively decreased the accumulation of 2,4-D compared with the non-treated control (Fig. 2A, B; see Supplementary Fig. S2A at *JXB* online). Surprisingly, application of the auxin efflux inhibitor NPA significantly increased accumulation of ^{3}H-2,4-D (Fig. 2C; see

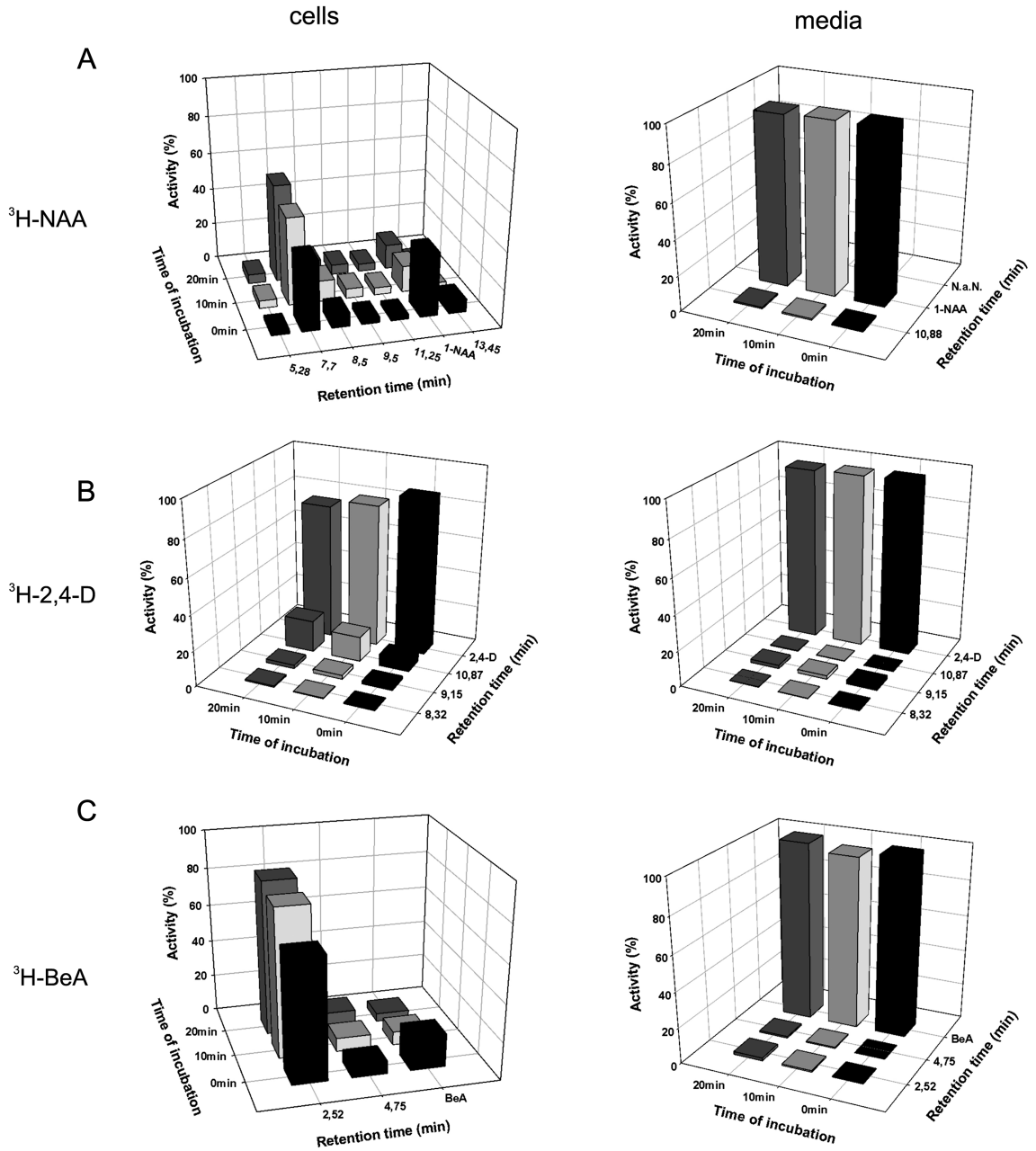

Fig. 1. Metabolism of ^{3}H-NAA, ^{3}H-2,4-D, and ^{3}H-BeA in tobacco BY-2 cells and in culture media. (A) NAA is rapidly metabolized to major metabolite M1 (identified as NAA glucosyl ester with a retention time of 7.7 min), which is predominant in the cells at 10 min and 20 min. No changes of NAA levels and only one minor metabolite peak were observed in the incubation medium, indicating that products of NAA metabolism (including the predominant NAA glucosyl ester) remained inside the cells. (B) 2,4-D is only partially metabolized to three unknown products. Thus the levels of 2,4-D slightly decreased during 20 min incubation, with a concurrent increase of an unknown metabolite at a retention time of 10.87 min. Levels of 2,4-D in the incubation medium remained constant and only three minor metabolites were observed, indicating that the products of 2,4-D metabolism also remained in the cells. (C) BeA was quickly metabolized to one predominant product at a retention time of 2.52 min (identified as BeA glucosyl ester) and one unknown minor product at a retention time of 4.75 min. A slight decrease of BeA content was observed in the incubation medium. Both metabolites were detected in the medium only as insignificant traces, indicating that these products remained in the cells. The percentages of individual peak activities were determined and normalized according to the corresponding activities in the total samples (100 %).

Supplementary Fig. S2B at *JXB* online). This indicates that a significant portion of ^{3}H-2,4-D can be actively transported out of the cells.

Since 2,4-D has been shown to be transported poorly *in planta* (Ito and Gray, 2006) and it was demonstrated to be a poor substrate for auxin efflux carriers ABCB1 and ABCB19 (Titapiwatanakun *et al.*, 2009), the activity of other types of NPA-sensitive auxin efflux transporters (Petrášek *et al.*, 2006; Yang and Murphy, 2009; Kubeš *et al.*, 2012) was probably reflected in our data.

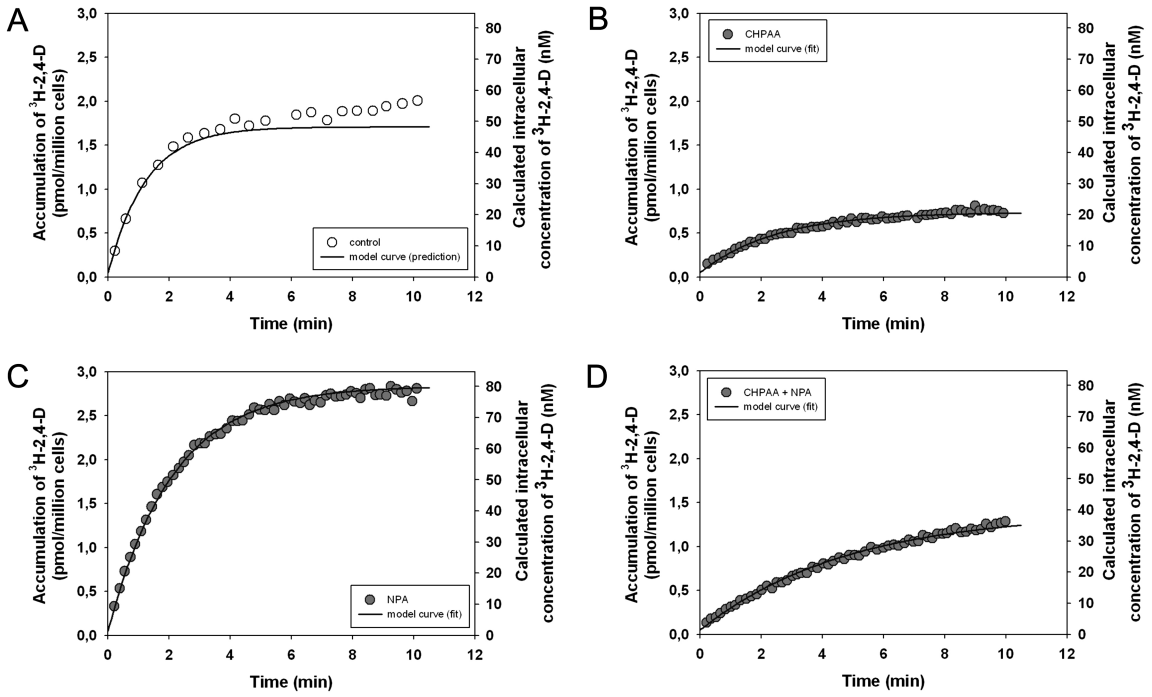

Fig. 2. Accumulation of ^{3}H-2,4-D measured in the presence of the auxin transport inhibitors CHPAA, NPA or their combination in tobacco BY-2 cells. (A) Accumulation of ^{3}H-2,4-D (2 nM) in the control (EtOH only). (B) Treatment with CHPAA (10 μM in EtOH) decreased 2,4-D accumulation by inhibiting the active auxin influx. (C) NPA (10 μM in EtOH) increased 2,4-D accumulation by inhibiting the active auxin efflux. (D) Combination of both inhibitors (CHPAA and NPA) revealed the net diffusion of 2,4-D into the cells. Corresponding model output curves reproducing (B, C, D) or predicting (A) ^{3}H-2,4-D accumulation are shown. Only one (the best fitting) accumulation data set (a single experimental run) is plotted in each graph for the sake of picture clarity. See Supplementary Fig. S2 at *JXB* online for complete plots of accumulation curves.

Furthermore, the combination of both CHPAA and NPA resulted in a strikingly slower rate of 2 nM ^{3}H-2,4-D accumulation in contrast to the accumulation in controls (Fig. 2D; see Supplementary Fig. S2C at *JXB* online). It seems that, under these conditions, CHPAA and NPA effectively blocked both influx and efflux carriers, and that the resulting slow 2,4-D accumulation curve reflected net diffusive uptake resulting from a combination of diffusive influx and diffusive efflux.

Altogether, these results further support 2,4-D as a suitable tool for probing cellular auxin transport since not only active influx of 2,4-D but also its active efflux takes part in 2,4-D accumulation.

Mathematical model of 2,4-D transport on a single cell level

To check if the proposed concept of auxin transport is valid and consistent with the experimental data and to establish auxin transport characteristics for a single cell, a mathematical model of 2,4-D transport was designed using the presented results to formulate its basic assumptions and quantitative experimental data on 2,4-D accumulation for its construction and validation. The model of 2,4-D transport was constructed with the following assumptions.

(i) BY-2 cell suspension consists of individual and identical cells of constant volume, and the number of the cells (suspension density) does not change during the accumulation assay

Obviously, all BY-2 cells in the cell population are neither identical, nor are they in the same phase of their development within the subculture period. Since a 2-d-old cell population was always used for the accumulation measurements, most of the cells were young cells in a similar phase of development, with a constant proportion of dividing and interphasic cells. So, the situation has been simplified here in that all cells in the population have the same capacity for auxin-transport processes.

(ii) Once inside the cell, 2,4-D is distributed homogeneously within the entire cell volume

Cell compartmentalization can hardly be neglected from the biological point of view, but experimental data do not require any inner cell compartments to be incorporated in the model and thus they do not even allow identification of any cell compartment-related parameters. Besides, the young cells used in accumulation assays have a high proportion of cytosol to other compartments.

(iii) 2,4-D is not metabolized in the cells within the 10 min of the accumulation assay

Our results (see above) have provided the evidence for such an assumption.

(iv) Number and activity of carriers do not change during the accumulation

The addition of 2 nM radiolabelled 2,4-D at the beginning of the accumulation assay is not expected to produce any changes in the activity of the PM auxin carriers, and the authors are not aware of any report that would question this assumption.

(v) The kinetics of auxin influx and efflux carriers is linear

Based on the results of Delbarre *et al.* (1996), auxin carriers do not exhibit saturating behaviour until micromolar concentrations of auxins are reached. Since the extracellular concentration of ^{3}H-2,4-D was 2 nM and its intracellular concentration did not exceed 100 nM, it is assumed that just the linear part of carrier kinetics applies under the conditions used. In other words, that the 2,4-D flux through particular types of carrier is linearly proportional to the concentration of 2,4-D in its source compartment, that is, extracellular concentration for influx and vice versa.

(vi) Carrier inhibitors block the activity of carriers entirely and do not affect other cellular characteristics

When CHPAA is applied, complete inhibition of the active auxin influx is assumed, as well as complete inhibition of the active auxin efflux in the case of NPA application. No changes in carrier localization were observed up to 30 min after CHPAA treatment (Laňková *et al.*, 2010), and only processes other than auxin transport might be affected at high NPA concentrations (Petrášek *et al.*, 2002, 2003; Dhonukshe *et al.*, 2005, 2008).

Various combinations of auxin carrier inhibitors were used to alter the experimental setup in order to obtain data for the characterization of respective participating transport mechanisms. When CHPAA and NPA were applied simultaneously, only the passive diffusion of ^{3}H-2,4-D contributed to its net uptake. Such data, therefore, allowed the values of 2,4-D diffusion parameters to be identified. Individual application of CHPAA or NPA enabled optimization of values for the efflux or influx parameters, respectively. Although the optimization could be performed in such a stepwise manner, an algorithm for simultaneous parameter optimization was employed instead to achieve greater precision (see the Materials and methods).

Besides the proper parameters of the model, a constant vertical offset was added to the model solution as another parameter and optimized to let the model compensate for auxin contaminating the cells surface and thus causing a shift of the accumulation curve. Nevertheless, the final value of the offset parameter provided by the optimization process was relatively low compared with the levels of ^{3}H-2,4-D accumulation (Table 1; Fig. 2; see Supplementary Fig. S2 at *JXB* online), suggesting that contamination of the cell surface is substantially less important than that observed earlier by Delbarre *et al.* (1996). The final parameter values (Table 1) were validated by simulating the course of control ^{3}H-2,4-D accumulation (i.e. accumulation without inhibitors), demonstrating that the model can predict the shape of accumulation curves under various experimental conditions (Fig. 2A). Plasma membrane properties for 2,4-D (Table 2) were calculated from 2,4-D-transport-parameter estimates according to Figs 3 and 4. Further details about the construction of the mathematical model are given in Figs 3 and 4.

Table 1. Optimized parameter values

Symbol	Parameter	Value	Unit
p_I	Intracellular fraction of protonated ^{3}H-2,4-D	5.56×10^{-5}	–
k_D	Diffusion parameter	40.8	s^{-1}
k_E	Efflux parameter	3.00×10^{-3}	s^{-1}
k_I	Influx parameter	2.44×10^{-1}	s^{-1}
offset	Apparent increase of ^{3}H-2,4-D accumulation	5.05×10^{-2}	pmol mil^{-1}. cells

Table 2. Calculated PM permeability and transport activities for 2,4-D

Symbol	Property	Value	Unit
k_{Diff}	Diffusive permeability	2.35×10^{-4}	m s^{-1}
k_{Eff}	Efflux carrier transport activity	1.73×10^{-8}	m s^{-1}
k_{Inf}	Influx carrier transport activity	1.41×10^{-6}	m s^{-1}

Discussion

The synthetic auxins NAA and 2,4-D represent useful tools for single-cell-based auxin transport studies because of the distinct specificity of auxin influx and efflux carriers, particularly in tobacco cells (Delbarre *et al.*, 1996; Petrášek *et al.*, 2006). Since some metabolic activity of tobacco cells especially towards NAA was reported earlier (Delbarre *et al.*, 1994, 1996), its metabolism in relation to the possible interference of metabolites formed with the processes of auxin transport was investigated first. The incubation of cells with radiolabelled NAA, 2,4-D or the non-auxin weak acid BeA revealed metabolic changes that were fastest for BeA and NAA. Glucosyl ester conjugates represented the major form of respective metabolites as shown for NAA in this work and also by Kai *et al.* (2007) for IAA. Such glucosyl ester conjugates or other auxin metabolites were not detected in the cultivation media and therefore did not seem to be substrates for the auxin efflux transporters. Assuming an easy accessibility of glucose in cells, these findings are consistent with reports about the importance of IAA conjugation and conjugate hydrolysis for the regulation of auxin homeostasis in mosses, hornworts, pteridophytes, and seed plants, in contrast to charophytes and liverworts where auxin regulation is controlled by the balance between the rates of biosynthesis and degradation (reviewed by Cooke *et al.*, 2002).

It has been shown here that auxin metabolites remain trapped inside cells. This finding has an important consequence for accumulation assays based on radiolabelled auxin. Because auxin molecules are labelled preferably on the ring structures, the label stays inside cells in the form of

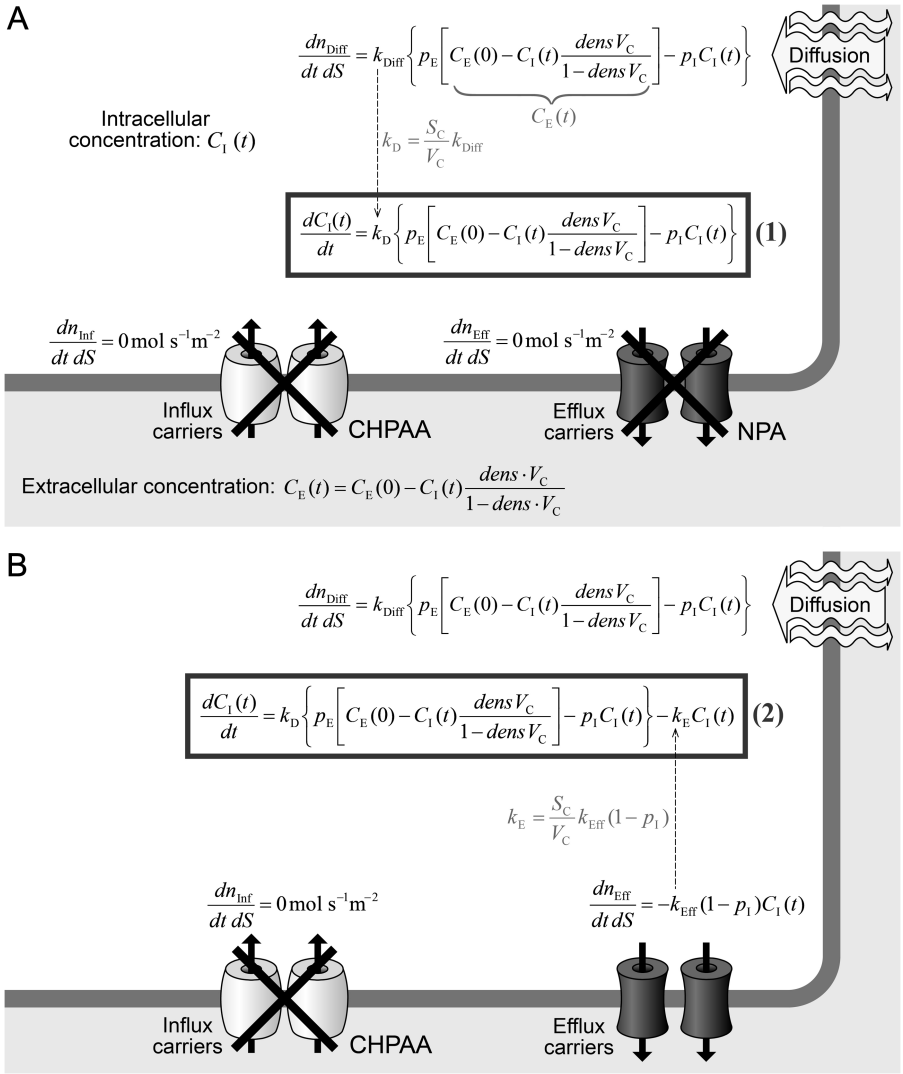

Fig. 3. Mathematical model of ^{3}H-2,4-D uptake by diffusion or both diffusion and efflux. (A) In the presence of CHPAA and NPA, it is assumed that the active influx and efflux, respectively, of ^{3}H-2,4-D are completely blocked. This is indicated in the scheme by expressions stating that the densities of the respective ^{3}H-2,4-D fluxes through the plasma membrane are null. Symbols indicate the amount of ^{3}H-2,4-D transported by influx carriers, dn_{Inf} , the amount of ^{3}H-2,4-D transported by efflux carriers, dn_{Eff} , expressed per unit of time, dt, and a unit of plasma membrane area, dS. The only non-zero flux of ^{3}H-2,4-D is, therefore, caused by diffusion. In a corresponding equation, dn_{Diff} represents the amount of passively transported ^{3}H-2,4-D, k_{Diff} is the diffusion permeability of plasma membrane, p_e and p_i represent the fraction (relative amount) of protonated (not dissociated) ^{3}H-2,4-D in the extracellular and intracellular space, respectively. Since both extracellular (C_E) and intracellular (C_I) concentrations of ^{3}H-2,4-D change during accumulation, the extracellular concentration was expressed using the initial extracellular concentration [$C_E(0)$], the intracellular concentration, cell suspension density (number of cells in units of suspension volume, *dens*), and cell volume (volume of a single cell, V_C) as indicated in the bottom of the scheme. This expression was then used to substitute for the ^{3}H-2,4-D extracellular concentration in the diffusion equation. To obtain the final differential equation of the model (1), the diffusion permeability of plasma membrane (k_{Diff}), which is a universal property of the membrane independent of cell dimensions, was replaced by the diffusion parameter (k_D), which is a rate-constant specific to the particular cell geometry represented by its volume (V_C) and surface area (S_C). (B) In the presence of CHPAA, the active ^{3}H-2,4-D influx is assumed to be completely inhibited, while the active efflux and diffusion of ^{3}H-2,4-D is unaffected. Therefore, the mathematical representation of ^{3}H-2,4-D flux by diffusion remains identical to the one derived in (A). In the case of the active efflux, the flux of ^{3}H-2,4-D is assumed to be proportional to the source (intracellular) concentration of dissociated ^{3}H-2,4-D (i.e. a linear kinetics of efflux carriers is assumed). The appropriate parameter—the auxin efflux carrier activity of the membrane (k_{Eff})—is transformed again into the cell-specific rate constant k_E, the efflux parameter, according to the same principle used for diffusion parameters described above in (A). The efflux parameter (k_E) is then used in the final differential equation (2) of the model.

auxin metabolite(s) and thus the real intracellular concentration of free (labelled) auxin is lower than expected. This implies that the true transport efficiency of PIN and/or ABCB auxin efflux transporters is even higher than previously assumed for auxins that are metabolized quickly. In the case of the widely used NAA, free ^{3}H-NAA represented

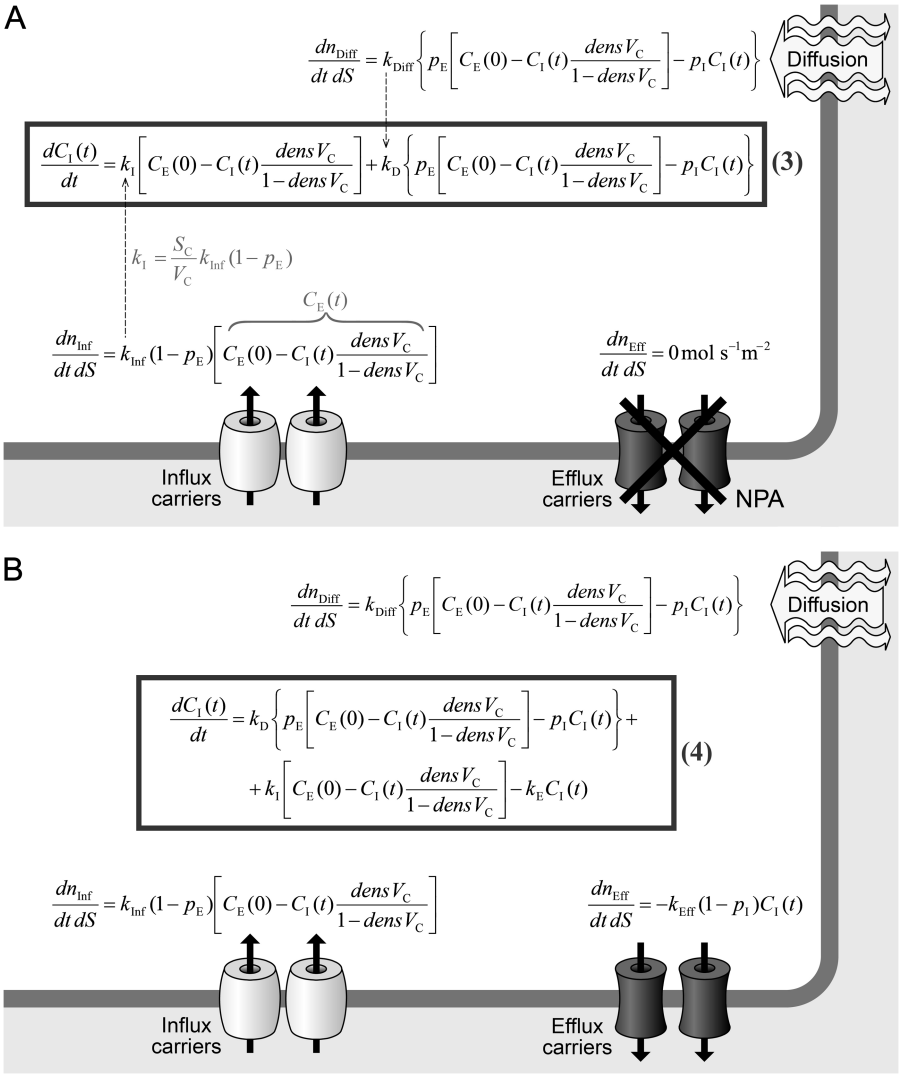

Fig. 4. Mathematical model of ^{3}H-2,4-D uptake by diffusion and influx, or by a combination of diffusion, influx and efflux. (A) In the presence of NPA, the active ^{3}H-2,4-D efflux is assumed to be completely inhibited, while the active influx and diffusion of ^{3}H-2,4-D are unaffected. Therefore, the mathematical representation of ^{3}H-2,4-D flux by diffusion remains unchanged. In the case of an active influx, the flux of ^{3}H-2,4-D is assumed to be proportional to the source (extracellular) concentration of dissociated ^{3}H-2,4-D (i.e. a linear kinetics of influx carriers is assumed). The appropriate parameter—influx carrier activity of the membrane (k_{Inf})—is again transformed into the cell-specific rate-constant k_I, the influx parameter, to obtain the final differential equation (3) of the model. (B) With no inhibitor present in the medium, all of the three transport mechanisms (i.e. diffusion, active influx, and active efflux) take part in the net uptake of ^{3}H-2,4-D by the cell. Therefore, the contributions of all these three processes are combined in the final differential equation (4) of the model.

from less than a half (*c.* 30 s after its addition to the cell suspension) to about a fifth (after 10 min) of overall accumulated radioactivity (Fig. 1), thus resulting in a 2–5-fold underestimation, respectively, of its efflux rate. In the case of the Michaelis–Menten efflux kinetics used by Delbarre *et al.* (1996), the half-saturation concentration would be affected in the opposite way (2–5-fold overestimated), while the parameter maximum transport capacity would remain unchanged. However, Delbarre *et al.* (1996) expressed the concentration of NAA corresponding to the half-saturation of NAA efflux as the extracellular NAA concentration, and so this value cannot be updated and discussed in the context of the experiments and the model presented here.

While the use of NAA as a tool for the precise characterization of auxin efflux depends on a detailed understanding of its metabolic changes, 2,4-D is metabolized fairly weakly and slowly. The high metabolic stability of 2,4-D is probably due to the substitution by two halogen (Cl) atoms, since halogenation of organic molecules has been considered to play an important role in their metabolic degradation, bioactivity, and conformation (Katekar 1979; Fero *et al.*, 2006). Therefore, 2,4-D was used in this work for probing the transport characteristics of auxin influx and efflux carriers. Although 2,4-D had previously been recognized as a poor substrate for efflux carriers (Delbarre *et al.*, 1996), in our experiments the application of the auxin efflux inhibitor NPA led to a pronounced increase in ^{3}H-2,4-D

levels, suggesting that 2,4-D is also a substrate for active auxin efflux. This is consistent with previous data showing that, in tobacco cell line VBI-0, 2,4-D could be partly transported across the plasma membrane via auxin efflux carriers (Petrášek *et al.*, 2002; Paciorek *et al.*, 2005), and that the over-expression of the *Arabidopsis* gene *PIN7* in BY-2 tobacco cells resulted in an increased efflux of 2,4-D (Petrášek *et al.*, 2006). The overall accumulation of ^{3}H-2,4-D after treatment with the specific auxin influx inhibitor CHPAA revealed an essential contribution of influx carriers to ^{3}H-2,4-D uptake, consistent with the previous conclusion (Delbarre *et al.*, 1996). Using the combination of inhibitors CHPAA and NPA for blocking auxin influx and efflux, respectively, the contribution of diffusion has been 'separated' from total 2,4-D accumulation. Although 2,4-D has been generally considered not to penetrate through PM via passive diffusion, our data show that the contribution of passive diffusion should not be overlooked (Fig. 5; see Supplementary Fig. S6 at *JXB* online).

The results of the ^{3}H-2,4-D accumulation experiments, together with their interpretation presented above, provide an image of short-term cellular transport of 2,4-D. On the basis of this image a mathematical model was constructed. The fact that the model can reproduce, and even successfully predict, the levels of 2,4-D accumulated by tobacco cells supports the proposed system, confirming its consistency and a fairly accurate agreement with the data. Moreover, optimization of the model produced estimates of crucial 2,4-D transport parameters such as diffusive permeability of the PM and transport activities of the efflux and influx carriers (Table 2).

Obviously, the values of these parameters are specific to the particular plant material and experimental conditions, and therefore cannot be taken as generally valid. Nevertheless, they can be discussed and to some extent also compared with analogous parameters stated elsewhere. Delbarre *et al.* (1996) presented Michaelis–Menten kinetic parameter values for 2,4-D influx from which an equivalent of our influx parameter (k_I) can be calculated. Assuming no carrier saturation whatsoever, this gives a value of 0.013 s^{-1}. This value corresponds to our 2,4-D influx parameter estimate (k_I=0.24 s^{-1}), pointing at some key aspects of different methodology. Since Delbarre *et al.* (1996) saturated the carriers with cold 2,4-D in order to measure their kinetics, the fact that they underestimated the efflux of 2,4-D was likely to interfere with the influx activity. Consequently, concurrent saturation of both auxin influx and efflux would decrease the significance of the observed saturable component (because the common portions of saturated influx and efflux would be mutually compensated, leaving just their difference visible). This could result in apparently lower participation of influx on overall 2,4-D accumulation. The simultaneously saturated portions of influx and efflux would then contribute to the non-saturable part of 2,4-D uptake. A part of this non-saturable component was interpreted by Delbarre *et al.* (1996) as cell surface contamination, which explains their surprisingly high value of this parameter. By contrast, parameter estimates and the sensitivity analysis in our model (Table S1; see Supplementary Fig. S5 at *JXB* online) render cell surface contamination insignificant.

When comparing our 2,4-D efflux and influx parameters (k_E=0.003 s^{-1} and k_I=0.24 s^{-1}) with each other, dominance of the influx activity over efflux of 2,4-D is evident (Fig. 5; see Supplementary Fig. S6 at *JXB* online). However, the intracellular concentration of 2,4-D rises very quickly and compensates a considerable portion of the massive difference between 2,4-D influx and efflux rate constants. For instance, at the state of equilibrium (to which the late phase of 2,4-D accumulation is relatively close) the intensity of active efflux corresponds to about 70% of the intensity of 2,4-D influx (Fig. 5).

It should be stressed that the assumption of homogeneous distribution of 2,4-D within the cells by neglecting inner cell compartments seriously limits the solidity of the efflux parameter estimate. This is because the retention of 2,4-D in an intracellular compartment would result in the

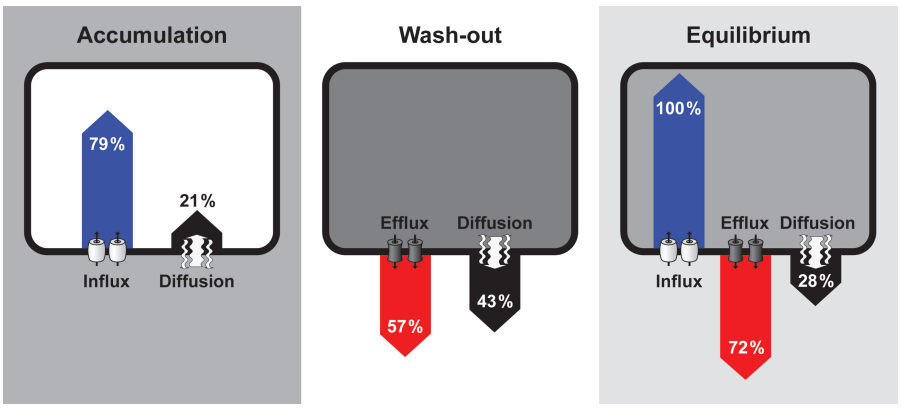

Fig. 5. Comparison of relative contribution of 2,4-D transport processes on a cellular level. The mathematical model predicts the relative contributions of the three distinct 2,4-D transport processes in the following model situations: initial phase of 2,4-D accumulation (2,4-D in the medium, no 2,4-D in cells), wash-out of accumulated 2,4-D to auxin-free medium, and a steadystate. Shades of grey represent 2,4-D concentrations in intracellular and extracellular space. Notice that, in the case of an equilibrium (2,4-D concentrations, both inside and outside the cell, do not change), the 2,4-D level is higher inside the cell.

difference between the actual cytoplasmic 2,4-D concentration and the modelled value, that was simply averaged over the cell volume. Therefore, a different value of the appropriate rate constant—the efflux parameter—would be necessary to simulate the observed flux. The extent of the bias of the present efflux parameter estimate could be assessed approximately by the change of the estimated value if a plant material with significantly less or more pronounced cellular compartmentalization is used. However, if suitable data directly reflecting cell compartmentalization are available in the future, the present model can be modified in an attempt to characterize the intracellular compartments such as the ER, which was proposed to play a role in intracellular auxin signalling (Mravec *et al.*, 2009; Wabnik *et al.*, 2011).

The estimate of intracellular fraction of protonated ^{3}H-2,4-D (p_I=5.56×10^{-5}) can be verified by calculating the appropriate value of intracellular pH according to the Henderson–Hasselbach equation. The resulting intracellular pH value of 7.15 is fairly plausible and thus supports the credibility of this parameter estimate. The issue of auxin-related pH dynamics links our model closely to the work by Steinacher *et al.* (2012), who specialized in this matter with their mathematical model of auxin-induced cell wall acidification. Although they were dealing with natural IAA, it is noteworthy that their model, which so far does not integrate any auxin transport data, could be supported by the experimentally assisted approach to the modelling of auxin transport presented here.

Taken together, a single-cell-based system of experimental–computational characterization of auxin transport is introduced. Mathematical modelling is used here as a tool for interpretation and validation of experimental data applying an 'analytical approach' to derive the model in direct relation to the data. This concept harvests new biological information from the data and, moreover, the model itself has a potential to produce parameter estimates and to complement existing models of hypothetical auxin transport regulation mechanisms.

Supplementary data

Supplementary data can be found at *JXB* online.

Supplementary Table S1. Table of known parameters and conditions.

Supplementary Fig. S1. Metabolism of ^{3}H-NAA, ^{3}H-2,4-D, ^{3}H-BeA in Xanthi tobacco cells and media at time 0 (approximately 20 s) and 10 min of incubation.

Supplementary Fig. S2. Complete plots of ^{3}H-2,4-D (2 nM) accumulation curves measured under the effects of the auxin transport inhibitors CHPAA, NPA, and their combination (10 μM in EtOH) in BY-2 tobacco cells.

Supplementary Fig. S3. Identification of the main NAA metabolite (NAA glucosyl ester).

Supplementary Fig. S4. Confirmation of the ester bond in the NAA major metabolite (identified as NAA glucosyl ester).

Supplementary Fig. S5. Sensitivity of model-data fit quality to parameter change.

Supplementary Fig. S6. Detailed simulation of the model accumulation assay.

Acknowledgements

The work was supported by the Ministry of Education, Youth and Sports of the Czech Republic project LC06034, by the Grant Agency of the Czech Republic, project P305/11/0797 and by project MSM6840770012 Trans-disciplinary Research in the Field of Biomedical Engineering II. We thank Dr Helena Lipavská for HPLC analysis of the hexose sample, Markéta Pařezová and Jana Stýblová for technical assistance, and Dr Jan Marc for critical reading.

References

Bayer EM, Smith RS, Mandel T, Nakayama N, Sauer M, Prusinkiewcz P, Kuhlemeier C. 2009. Integration of transport-based models for phyllotaxis and midvein formation. *Genes and Development* **23,** 373–384.

Cho M, Lee SH, Cho HT. 2007. P-glycoprotein4 displays auxin efflux transporter-like action in Arabidopsis root hair cells and tobacco cells. *The Plant Cell* **19,** 3930–3943.

Cooke TJ, Poli D, Sztein AE, Cohen JD. 2002. Evolutionary patterns in auxin action. *Plant Molecular Biology* **49,** 319–338.

Davies PJ, ed. 2010. *The plant hormones: biosynthesis, signal transduction, action!*, 3rd edn. Dordrecht, The Netherlands: Springer.

Delbarre A, Muller P, Imhoff V, Guern J. 1996. Comparison of mechanisms controlling uptake and accumulation of 2,4-dichlorophenoxy acetic acid, naphthalene-1-acetic acid, and indole-3-acetic acid in suspension-cultured tobacco cells. *Planta* **198,** 532–541.

Delbarre A, Muller P, Imhoff V, Morgat JL, Barbier-Brygoo H. 1994. Uptake, accumulation and metabolism of auxins in tobacco leaf protoplasts. *Planta* **195,** 159–167.

Dhonukshe P, Kleine-Vehn J, Friml J. 2005. Cell polarity, auxin transport, and cytoskeleton-mediated division planes: who comes first? *Protoplasma* **226,** 67–73.

Dhonukshe P, Tanaka H, Goh T, *et al*. 2008. Generation of cell polarity in plants links endocytosis, auxin distribution and cell fate decisions. *Nature* **456,** 962–975.

Dobrev PI, Havlíček L, Vágner M, Malbeck J, Kamínek M. 2005. Purification and determination of plant hormones auxin and abscisic acid using solid phase extraction and two-dimensional high performance liquid chromatography. *Journal of Chromatography A* **1075,** 159–166.

Dobrev PI, Kamínek M. 2002. Fast and efficient separation of cytokinins from auxin and abscisic acid and their purification using mixed-mode solid-phase extraction. *Journal of Chromatography A* **950,** 21–29.

Ferro N, Gallegos A, Bultinck P, Jacobsen HJ, Dorca R, Reinard T. 2006. Coulomb and overlap self-similarities: a comparative

selectivity analysis of structure–function relationships for auxin-like molecules. *Journal of Chemical Information and Modeling* **46,** 1751–1762.

Feugier FG, Mochizuki A, Iwasa Y. 2005. Self-organization of the vascular system in plant leaves: inter-dependent dynamics of auxin flux and carrier proteins. *Journal of Theoretical Biology* **236,** 366–375.

Fujita H, Mochizuki A. 2006. Pattern formation by the positive feedback regulation between flow of diffusible signal molecule and localization of its carrier. *Journal of Theoretical Biology* **241,** 541–555.

Gailweiler L, Guan C, Muller A, Wisman E, Mendgen K, Yephremov A, Palme K. 1998. Regulation of polar auxin transport by AtPIN1 in Arabidopsis vascular tissue. *Science* **282,** 2226–2230.

Gamborg OL, Miller RA, Ojima K. 1968. Nutrient requirements of suspension cultures of soybean root cells. *Experimental Cell Research* **15,** 148–151.

Garnett P, Steinacher A, Stepney S, Clayton R, Leyser O. 2010. Computer simulation: the imaginary friend of auxin transport biology. *Bioessays* **32,** 828–835.

Geisler M, Murphy AS. 2006. The ABC of auxin transport: the role of p-glycoproteins in plant development. *FEBS Letters* **580,** 1094–1102.

Goldsmith MHM. 1977. The polar transport of auxin. *Annual Review of Plant Physiology* **28,** 439–478.

Heisler MG, Hamant O, Krupinski P, Uyttewaal M, Ohno C, Jönsson H, Traas J, Meyerowitz EM. 2010. Alignment between PIN1 polarity and microtubule orientation in the shoot apical meristem reveals a tight coupling between morphogenesis and auxin transport. *PLoS Biolology* **8,** e1000516. doi:10.1371/journal.pbio.1000516.

Heisler MG, Jönsson H. 2006. Modeling auxin transport and plant development. *Journal of Plant Growth Regulation* **25,** 302–312.

Imhoff V, Muller P, Guern J, Delbarre A. 2000. Inhibitors of the carrier-mediated influx of auxin in suspension-cultured tobacco cells. *Planta* **210,** 580–588.

Ito H, Gray WM. 2006. A gain-of-function mutation in the Arabidopsis pleiotropic drug resistance transporter PDR9 confers resistance to auxinic herbicides. *Plant Physiology* **142,** 63–74.

Jönsson H, Heisler MG, Shapiro BE, Meyerowitz EM, Mjolsness E. 2006. An auxin-driven polarized transport model for phyllotaxis. *Proceedings of the National Academy of Sciences, USA* **103,** 1633–1638.

Kai K, Nakamura S, Wakasa K, Miyagawa H. 2007. Facile preparation of deuterium-labeled indole-3-acetic acid (IAA) and its metabolites to quantitatively analyze the disposition of exogenous IAA in *Arabidopsis thaliana*. *Bioscience Biotechnology and Biochemistry* **71,** 1946–1954.

Katekar GF. 1979. Auxins: nature of the receptor-site and molecular requirements for auxin activity. *Phytochemistry* **18,** 223–233.

Kramer EM. 2008. Computer models of auxin transport: a review and commentary. *Journal of Experimental Botany* **59,** 45–53.

Kramer EM, Bennett MJ. 2006. Auxin transport: A field in flux. *Trends in Plant Science* **11,** 382–386.

Kubeš M, Yang H, Richter GL, *et al*. 2012. The Arabidopsis concentration-dependent influx/efflux transporter ABCB4 regulates cellular auxin levels in the root epidermis. *The Plant Journal,* (in press). doi: 10.1111/j.1365-313X.2011.04818.x.

Laňková M, Smith RS, Pešek B, Kubeš M, Zažímalová E, Petrášek J, Hoyerová K. 2010. Auxin influx inhibitors 1-NOA, 2-NOA, and CHPAA interfere with membrane dynamics in tobacco cells. *Journal of Experimental Botany* **61,** 3589–3598.

Leyser O. 2011. Auxin, self-organisation, and the colonial nature of plants. *Current Biology* **21,** 331–337.

Ludwig-Muller J. 2011. Auxin conjugates: their role for plant development and in the evolution of land plants. *Journal of Experimental Botany* **62,** 1757–1773.

Merks RMH, Van de Peer Y, Inzé D, Beemster GTS. 2007. Canalization without flux sensors: a traveling-wave hypothesis. *Trends in Plant Science* **12,** 384–390.

Mitchison GJ. 1980*a*. A model for vein formation in higher plants. *Proceedings of the Royal Society of London, Series B* **207,** 79–109.

Mitchison GJ. 1980*b*. The dynamics of auxin transport. *Proceedings of the Royal Society of London, Series B* **209,** 489–511.

Mitchison GJ, Hanke DE, Sheldrake AR. 1981. The polar transport of auxin and vein patterns in plants. *Philosophical Transactions of the Royal Society of London, Series B* **295,** 461–471.

Mravec J, Skůpa P, Bailly A, *et al*. 2009. Subcellular homeostasis of phytohormone auxin is mediated by the ER-localized PIN5 transporter. *Nature* **459,** 1136–1140.

Muller JF, Goujaud J, Caboche M. 1985. Isolation *in vitro* of naphthalene-acetic-tolerant mutants of *Nicotiana tabacum*, which are impaired in root morphogenesis. *Molecular and General Genetics* **199,** 194–200.

Nagata T, Nemoto Y, Hasezava S. 1992. Tobacco BY-2 cell line as the 'Hela' cell in the cell biology of higher plants. *International Review of Cytology* **132,** 1–30.

Normanly J, Slovin JP, Cohen JD. 2010. Hormone biosynthesis, metabolism and its regulation. In: Davies PJ, ed. *Plant hormones: biosynthesis, signal transduction, action!* 3rd edn. Dordrecht, The Netherlands: Springer, 36–62.

Paciorek T, Zažímalová E, Ruthardt N, *et al*. 2005. Auxin inhibits endocytosis and promotes its own efflux from cells. *Nature* **435,** 1251–1256.

Parry G, Delbarre A, Marchant A, Swarup R, Napier R, Perrot-Rechenmann C, Bennett MJ. 2001*a*. Novel auxin transport inhibitors phenocopy the auxin influx carrier mutation aux1. *The Plant Journal* **25,** 399–406.

Parry G, Marchant A, May S, *et al*. 2001*b*. Quick on the uptake: Characterization of a family of plant auxin influx carriers. *Journal of Plant Growth Regulation* **20,** 217–225.

Peer WA, Blakeslee JJ, Yang H, Murphy AS. 2011. Seven things we think we know about auxin transport. *Molecular Plant* **4,** 487–504.

Peer WA, Murphy AS. 2007. Flavonoids and auxin transport: modulators or regulators? *Trends in Plant Science* **12,** 556–563.

Petrášek J, Černá A, Schwarzerová K, Elčkner M, Morris DA, Zažímalová E. 2003. Do phytotropins inhibit auxin efflux by impairing vesicle traffic? *Plant Physiology* **131,** 254–263.

Petrášek J, Elčkner M, Morris DA, Zažímalová E. 2002. Auxin efflux carrier activity and auxin accumulation regulate cell division and polarity in tobacco cells. *Planta* **216,** 302–308.

Petrášek J, Friml J. 2009. Auxin transport routes in plant development. *Development* **136,** 2675–2688.

Petrášek J, Mravec J, Bouchard R, *et al*. 2006. PIN proteins perform a rate-limiting function in cellular auxin efflux. *Science* **312,** 914–918.

Rahman A, Ahamed A, Amakawa T, Goto N, Tsurumi S. 2001. Chromosaponin I specifically interacts with AUX1 protein in regulating the gravitropic response of arabidopsis roots. *Plant Physiology* **125,** 990–1000.

Raven J. 1975. Transport of indoleacetic acid in plant cells in relation to pH and electrical potential gradients, and its significance for polar IAA transport. *New Phytologist* **74,** 163–172.

Rubery P. 1990. Phytotropins-receptors and endogenous ligands. *Hormone perception and signal transduction in animals and plants*. Book Series. *Symposia of the Society for Experimental Biology* **44,** 119–146.

Rubery P, Sheldrake A. 1974. Carrier-mediated auxin transport. *Planta* **118,** 101–121.

Sachs T. 1969. Polarity and the induction of organized vascular tissues. *Annals of Botany* **33,** 263–275.

Shitan N, Bazin I, Dan K, Obata K, Kigawa K, Ueda K, Sato F, Forestier C, Yazaki K. 2003. Involvement of CjMDR1, a plant multidrug-resistance-type ATP-binding cassette protein, in *alkaloid transport in Coptis japonica*. *Proceedings of the National Academy of Sciences, USA* **100,** 751–756.

Smith RS, Bayer EM. 2009. Auxin transport-feedback models of patterning in plants. *Plant, Cell and Environment* **32,** 1258–1271.

Smith RS, Guyomarch S, Mandel T, Reinhardt D, Kuhlemeier C, Prusinkiewicz P. 2006. A plausible model of phyllotaxis. *Proceedings of the National Academy of Sciences, USA* **103,** 1301–1306.

Steinacher A, Leyser O, Clayton RH. 2012. A computational model of auxin and pH dynamics in a single plant cell. *Journal of Theoretical Biology* **296,** 84–94.

Stoma S, Lucas M, Chopard J, Schaedel J, Traas J, Godin C. 2008. Flux-based transport enhancement as a plausible unifying mechanism for auxin transport in meristem development. *PLoS Computational Biology* **4,** e1000207.

Terasaka K, Blakeslee JJ, Titapiwatanakun B, *et al*. 2005. PGP4, an ATP binding cassette P-glycoprotein, catalyzes auxin transport in *Arabidopsis thaliana* roots. *The Plant Cell* **17,** 2922–2939.

Titapiwatanakun B, Blakeslee JJ, Bandyopadhyay A, *et al*. 2009. ABCB19/PGP19 stabilises PIN1 in membrane microdomains in Arabidopsis. *The Plant Journal* **57,** 27–44.

Titapiwatanakun B, Murphy AS. 2009. Post-transcriptional regulation of auxin transport proteins: cellular trafficking, protein phosphorylation, protein maturation, ubiquitination, and membrane composition. *Journal of Experimental Botany* **60,** 1093–1097.

Tromas A, Paponov I, Perrot-Rechenmann C. 2010. AUXIN BINDING PROTEIN 1: functional and evolutionary aspects. *Trends in Plant Science* **15,** 436–446.

Wabnik K, Govaerts W, Friml J, Kleine-Vehn J. 2011. Feedback models for polarized auxin transport: an emerging trend. *Molecular BioSystems* **7,** 2352–2359.

Wabnik K, Kleine-Vehn J, Balla J, Sauer M, Naramoto S, Reinöhl V, Merks RMH, Goaverts W, Friml J. 2010. Emergence of tissue polarization from synergy of intracellular and extracellular auxin signaling. *Molecular Systems Biology* **6,** 447.

Yamamoto M, Yamamoto KT. 1998. Differential effects of 1-naphthalene acetic acid, indole-3-acetic acid and 2,4-dichlorophenoxyacetic acid on the gravitropic response of roots in an auxin resistant mutant of Arabidopsis *Aux1*. *Plant and Cell Physiology* **39,** 660–664.

Yang HB, Murphy AS. 2009. Functional expression and characterization of Arabidopsis ABCB AUX 1 and PIN auxin transporters in *Schizosaccharomyces pombe*. *The Plant Journal* **59,** 179–191.

Zažímalová E, Murphy A, Yang H, Hoyerová K, Hošek P. 2010. Auxin transporters: why so many? *Cold Spring Harbor Perspectives in Biology* **2,** a001552.